Daniel S. Pilch[1,2]
Malvika Kaul[1]
Christopher M. Barbieri[1]
John E. Kerrigan[2,3]
[1] *Department of Pharmacology, University of Medicine and Dentistry of New Jersey–Robert Wood Johnson Medical School, 675 Hoes Lane, Piscataway, NJ 08854-5635*

[2] *The Cancer Institute of New Jersey, New Brunswick, NJ 08901*

[3] *Division of Academic Computing, University of Medicine and Dentistry of New Jersey, Piscataway, NJ 08854*

Thermodynamics of Aminoglycoside–rRNA Recognition

Received 18 February 2003; accepted 18 February 2003

Abstract: *2-Deoxystreptamine (2-DOS) aminoglycosides are a family of structurally related broad-spectrum antibiotics that are used widely in the treatment of infections caused by aerobic Gram-negative bacilli. Their antibiotic activities are ascribed to their abilities to bind a highly conserved A site in the 16 S rRNA of the 30 S ribosomal subunit and interfere with protein synthesis. The abilities of the 2-DOS aminoglycosides to recognize a specific subdomain of a large RNA molecule make these compounds archetypical models for RNA-targeting drugs. This article presents a series of calorimetric, spectroscopic, osmotic stress, and computational studies designed to evaluate the thermodynamics (ΔG, ΔH, ΔS, ΔC_p) of aminoglycoside–rRNA interactions, as well as the hydration changes that accompany these interactions. In conjunction with the current structural database, the results of these studies provide important insights into the molecular forces that dictate and control the rRNA binding affinities and specificities of the aminoglycosides. Significantly, identification of these molecular driving forces [which include binding-linked drug protonation reactions, polyelectrolyte contributions from counterion release, conformational changes, hydration effects, and molecular interactions (e.g., hydrogen bonds and van der Waals interac-*

Correspondence to: Daniel S. Pilch; email: pilchds@umdnj.edu
Contract grant sponsor: American Cancer Society (ACS) and NIH
Contract grant number: RSG-99-153-04-CDD (ACS) and RR15959-01 (NIH)
Biopolymers, Vol. 70, 58–79 (2003)

tions)], as well as the relative magnitudes of their contributions to the binding free energy, could not be achieved by consideration of structural data alone, highlighting the importance of acquiring both *thermodynamic and structural information for developing a complete understanding of the drug–RNA binding process. The results presented here begin to establish a database that can be used to predict, over a range of conditions, the relative affinity of a given aminoglycoside or aminoglycoside mimetic for a targeted RNA site vs binding to potential competing secondary sites. This type of predictive capability is essential for establishment of a rational design approach to the development of new RNA-targeted drugs.* © 2003 Wiley Periodicals, Inc. Biopolymers 70: 58–79, 2003

Keywords: *drug–RNA interactions; calorimetry; major groove binders; binding-induced drug protonation; heat capacity; molecular dynamics; osmotic stress; hydration; free energy; polyelectrolyte effect*

INTRODUCTION

RNA is a versatile molecule that, like proteins, is capable of folding into a broad range of different structures and conformations, which can serve as specific recognition elements for small molecules. The targeting of small molecules to specific RNA structures and sequences offers the potential for modulating the biological activities of the host RNA molecules, and in turn, the development of effective pharmaceutical agents. Realizing this potential requires an intimate understanding of small molecule–RNA binding interactions. Such information is critical not only for defining mechanism of action, but also for the development of a rational approach to the design of new compounds that exhibit desired activities. Small molecule–RNA interactions are also of interest from a more fundamental point of view in that they offer a well-defined model system for defining the factors that are important in the selective recognition of RNA. Numerous cellular and viral biochemical processes that are critical for replication and gene expression involve specific protein–RNA interactions. Thus, there is considerable interest in understanding the general principles that contribute to selective RNA recognition. Thermodynamic studies of small molecule–RNA interactions can provide insight into the molecular forces that dictate and control RNA binding affinity and specificity.

The high-resolution structural database of drug–RNA complexes has grown considerably in recent years, due, in part, to advances in NMR and crystallographic methodologies as well as in both enzymatic and chemical synthesis of RNA. The structures of more than 40 drug–RNA complexes have now been deposited in the Nucleic Acid Data Base and Protein Data Bank.[1,2] This wealth of structural data has provided enormous insight into the molecular basis of observed binding specificities. One of the features to emerge from the structural database is that many small molecule–RNA interactions are accompanied by conformational changes,[3–16] a feature that complicates attempts to correlate structure with binding affinity. The contributions of hydration effects to binding affinity and specificity are also difficult to ascertain from structural information alone. While extremely valuable, high-resolution structural information does not provide a complete understanding of the small molecule–RNA interaction. Such an understanding also requires detailed kinetic and thermodynamic information about the complexes. In this connection, recent attempts at structure-based drug design have met with only modest success, due, in large part, to a poor understanding of the thermodynamic forces governing the binding process. Using aminoglycoside antibiotics as models, one of the goals of this article is to illustrate how thermodynamic and structural information can be integrated to provide a more complete understanding of the molecular driving forces for drug–RNA complex formation.

The aminoglycosides are a structurally related group of broad-spectrum antibiotics that are used widely in the treatment of infections caused by aerobic Gram-negative bacilli.[17] They have predictable pharmacokinetic properties and often act in synergy with other antibiotics, two appealing characteristics that bolster their clinical value.[17,18] The aminoglycosides target a highly conserved sequence in the 16 S rRNA of the 30 S ribosomal subunit in prokaryotes.[19,20] This conserved RNA sequence forms the site, termed the A site, at which the interaction between the anticodon of the aminoacyl–tRNA and the mRNA codon occurs.[21] The antibiotic activities of the aminoglycosides are attributed to their abilities to interfere with this crucial step in the translation process.[20] The deleterious impact of aminoglycosides on protein synthesis includes both a reduction in translational fidelity as well as inhibition of the translocation step.[20,22,23] The abilities of the aminoglycosides to recognize a specific subdomain of a large RNA mol-

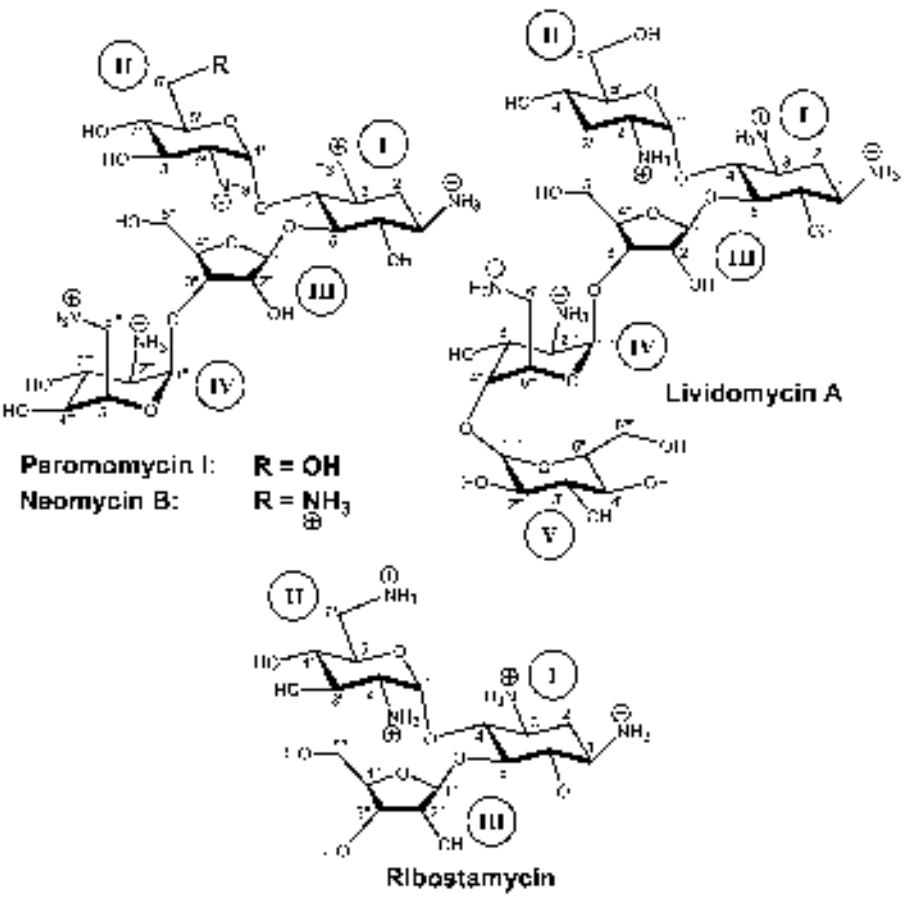

FIGURE 1 Structures of paromomycin I, neomycin B, lividomycin A, and ribostamycin in their fully protonated cationic states, with the atomic and ring numbering systems denoted in Arabic and Roman numerals, respectively. In each of the drugs depicted, ring I is 2-DOS.

ecule make these compounds archetypical models for RNA-targeting drugs. In this connection, the aminoglycosides represent the paradigm for drug–ribosome interactions, and information gleaned from their study has relevance to other ribosome-directed antibiotics of acute clinical importance.

Aminoglycosides derive their name from their structures, which consist of amino sugars and cyclitols that are linked glycosidically. Reported pK_a values for aminoglycoside amino groups range from approximately 5.7 to 9.5.[24–28] Thus, aminoglycosides exist as oligocations at physiologically relevant values of pH. All of the clinically useful aminoglycosides contain a highly substituted aminocyclitol as either a central or terminal ring. This ring is streptidine in streptomycin, while being 2-deoxystreptamine (2-DOS) in the other aminoglycosides. There are two major classes of 2-DOS aminoglycosides, the 4,5-disubstituted 2-DOS class, which includes neomycin B, paromomycin I, lividomycin A, and ribostamycin (see structures in Figure 1), and the 4,6-disubstituted 2-DOS class, which includes tobramycin, kanamycins A and B, amikacin, and the gentamicins.

The central potion of the 16 S rRNA A site contains an asymmetric internal loop formed by nucleotides A1408, A1492, and A1493 (see Figure 2). Footprinting studies have indicated that this region of 16 S rRNA is essentially free of contacts with ribosomal proteins,[29] an observation later confirmed by the recently reported crystal structure of the 30 S ribosomal subunit of *Thermus thermophilus*.[30,31] In the aggregate, these results suggested that appropriately designed RNA oligonucleotides might be able to recapitulate the local structure and/or conformation that exists in the decoding region A site within the ribosome. The Puglisi group took such a reductionist approach by designing a 27-mer hairpin oligonucleotide (whose sequence and secondary structure are shown in Figure 2) intended to mimic the decoding region A site of *Escherichia coli* 16 S rRNA.[9,32] Significantly, they demonstrated that the pattern of aminoglycoside-induced protection of the RNA bases

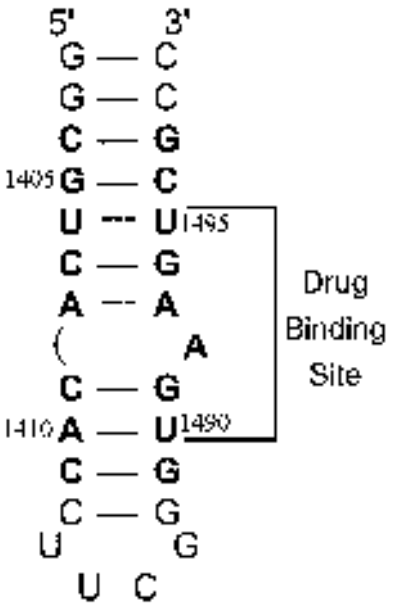

FIGURE 2 Secondary structure of the 27-mer A site model RNA oligonucleotide, as derived by NMR.[9] Watson–Crick base pairs are denoted by solid lines, while noncanonical base pairs are denoted by dashed lines. Bases present in *E. coli* 16 S rRNA are depicted in bold face, and are numbered as they are in 16 S rRNA. The aminoglycoside binding site, as revealed by NMR and footprinting studies,[9,32,76] is as indicated.

from methylation by dimethylsulfate (DMS) was virtually identical in the oligonucleotide construct as it was in the 30 S ribosomal subunit.[9,32]

To date, only a handful of structural studies probing the interactions of aminoglycosides with rRNA sequences have been reported.[9,11,14–16,33] In the first set of these studies, Puglisi and co-workers used NMR techniques to determine the solution structure of the 27-mer A site model oligonucleotide shown in Figure 2, as well as those of its complexes with paromomycin I[9] and gentamicin C1a.[33] These studies revealed the first insights into some of the key molecular interactions that underlie the specificities of representative members of both the 4,5- and 4,6-disubstituted 2-DOS classes of aminoglycosides for the rRNA A site. Some of the key structural features to emerge from these studies are summarized as follows: (a) Both drugs bind in the major groove of the RNA at the site of the internal loop formed by A1408, A1492, and A1493 (Figure 2). (b) Both drugs induce a similar conformational change in the RNA, which includes a displacement of A1492 and A1493 towards the minor groove by approximately 3 and 4 Å, respectively. (c) The drugs bind in a pocket created, in part, by the displacement of A1492 and A1493 where they form an array of hydrogen-bonding, van der Waals, and electrostatic contacts with the host RNA.

Subsequent to the NMR studies noted above, Ramakrishnan and co-workers reported a crystal structure at 3.0 Å resolution of the 30 S ribosomal subunit of *T. thermophilus* in complex with paromomycin I.[30] Significantly, this structure revealed the same basic features as described above for the complex between paromomycin I and the A site model oligonucleotide, with the exception that the extents to which A1492 and 1493 were displaced toward the minor groove were greater in the crystal structure. The similarities between the structures of the 30 S ribosomal subunit and the A site model oligonucleotide in complex with paromomycin I underscore the usefulness and validity of the oligonucleotide model system. Westhof and co-workers have recently reported the crystal structures of A-site model oligonucleotides in complex with paromomycin I and tobramycin.[14,16] These structures emulate the global features revealed by the crystal structure of the paromomycin I complex with the 30 S ribosomal subunit, but also reveal additional drug–RNA contacts by virtue of their superior resolution (≈2.5 Å). One of the more significant contributions of these latter crystal structures was the indication of the specific participation of water molecules in aminoglycoside–rRNA recognition.[14,16]

The studies reported here are intended to provide thermodynamic information that can be integrated with the structural picture described above to enhance our understanding of the molecular forces that contribute to the rRNA binding affinities and specificities of the aminoglycosides. Such an understanding is required to establish a database that can be used to predict, over a range of conditions, the relative affinity of a given aminoglycoside or aminoglycoside mimetic for the targeted RNA site vs binding to potential competing secondary sites (e.g., other looped or nonlooped duplex RNA regions). This type of predictive capability, in turn, facilitates the rational design approach to the development of new RNA-targeted drugs.

pH DEPENDENCE OF AMINOGLYCOSIDE–rRNA RECOGNITION

One of the hallmarks of aminoglycoside–RNA interactions is the pH dependence of the RNA binding properties.[28,34,35] In this connection, we have shown that pH modulates the extent to which aminoglycosides thermally stabilize the host RNA (ΔT_m) as well as the observed binding energetics.[28,35] Specifically,

increasing pH results in a concomitant decrease in ΔT_m and observed binding free energy (ΔG_{obs}). In addition, the observed binding enthalpy (ΔH_{obs}) becomes more exothermic (favorable), while the observed entropic contribution to binding ($T\Delta S_{obs}$) becomes less favorable.[35] Thus, the pH-induced reduction in ΔG_{obs} is entirely entropic in origin.

At pH 5.5, Aminoglycoside–rRNA Complexation is Independent of Protonation or Deprotonation Effects

We have recently reported the pK_a values of the amino groups in paromomycin I, neomycin B, and lividomycin A sulfate, as determined by ^{15}N-NMR.[28] Hereafter, we will refer to these three drugs as paromomycin, neomycin, and lividomycin, respectively. Note that the pK_a values we have determined range from 6.92 to 9.51.[28] Thus, at pH 5.5, all three drugs are essentially fully protonated. At this pH value, we probed for coupled protonation or deprotonation reactions to the complexation of the three drugs with the A site model RNA oligonucleotide shown in Figure 2 using isothermal titration calorimetry (ITC) in the presence of two different buffers (cacodylate and 2-[N-morpholino]ethanesulfonic acid, or MES) that exhibit differing heats of ionization (−0.47 and +3.71 kcal/mol, respectively). If RNA complexation were linked to the uptake or release of protons, then the observed binding enthalpies (ΔH_{obs}) would differ in the two buffers. Figure 3 shows representative ITC profiles resulting from the injection of paromomycin into a solution of A site RNA oligonucleotide in cacodylate (A) and MES (B) buffers. Each of the heat burst curves in Figures 3A and B corresponds to a single drug injection. The areas under these heat burst curves were determined by integration to yield the associated injection heats. These injection heats were corrected by subtraction of the corresponding dilution heats derived from the injection of identical amounts of drug into buffer alone. Figures 3C and D show the resulting corrected injection heats plotted as a function of the [drug]/[duplex] ratio. The binding parameters that emerged from the fits of these ITC profiles are summarized in Table I. Note that the values of ΔH_{obs} are essentially identical in the two buffers (−2.8 ± 0.1 kcal/mol in cacodylate buffer and −2.9 ± 0.1 kcal/mol in MES buffer), an observation indicative of an absence of binding-linked protonation effects at pH 5.5. Likewise, the association constants (K_a) determined in the two buffers are also similar [$(3.7 \pm 0.7) \times 10^7 M^{-1}$ in cacodylate buffer and $(3.8 \pm 1.3) \times 10^7 M^{-1}$ in MES buffer]. Thus, the RNA binding profiles of paromomycin sulfate acquired at pH 5.5 and summarized in Table I reflect binding parameters (e.g., ΔH and K_a) that are intrinsic to the drug–RNA interaction and do not include contributions from protonation or deprotonation effects. Neomycin and lividomycin sulfate exhibited a similar binding behavior at pH 5.5, with their values of ΔH_{obs} being −4.2 and −5.7 kcal/mol, respectively.

At pH Values >5.5, Aminoglycoside–rRNA Complexation is Coupled to Drug Protonation

Recall that the pK_a values of the amino groups in paromomycin, neomycin, and lividomycin sulfate range from 6.92 to 9.51. Thus, increasing pH values above 5.5 will reduce the extent to which the amino groups on these drugs are protonated. The protonation of NH_2 groups, such as the 2-NH_2 group on D-glucosamine and the α-amino groups of amino acids, are known exothermic reactions. Such protonation events, while being enthalpically favorable, are entropically costly. Hence, it is likely that the pH dependence of ΔH_{obs} and $T\Delta S_{obs}$ noted above reflects binding-induced protonation of one or more drug NH_2 groups. In this connection, we sought to determine whether the pH dependence of the observed aminoglycoside–RNA binding properties described above reflects a linkage between drug binding and the release or uptake of protons. We conducted ITC experiments over a range of pH values using buffers that differ with respect to their heats of ionization (ΔH_{ion}). Thus, if the pH dependence of ΔH_{obs} reflects binding-induced uptake or release of protons, then its value at a given pH should vary with the ΔH_{ion} value of the buffer. Furthermore, the number of protons linked to binding at a specific pH (Δn), as well as the intrinsic binding enthalpy (ΔH_{int}), a value that differs from ΔH_{obs} in that it excludes enthalpic contributions from ionization of the buffer, can be determined by simultaneous solution of the following two equations[36]:

$$\Delta H_{obs1} = \Delta H_{int} + \Delta H_{ion1}\Delta n \quad (1a)$$

$$\Delta H_{obs2} = \Delta H_{int} + \Delta H_{ion2}\Delta n \quad (1b)$$

In these equations, the numerical subscripts refer to the different buffers. A positive value of Δn is indicative of a net uptake of protons, while a negative value of Δn is indicative of a net release of protons.

Figure 4 shows representative ITC profiles resulting from the injection of paromomycin sulfate into a solution of A site RNA oligonucleotide in bicine (A and C) and N-tris[hydroxymethyl]methyl-3-amin-

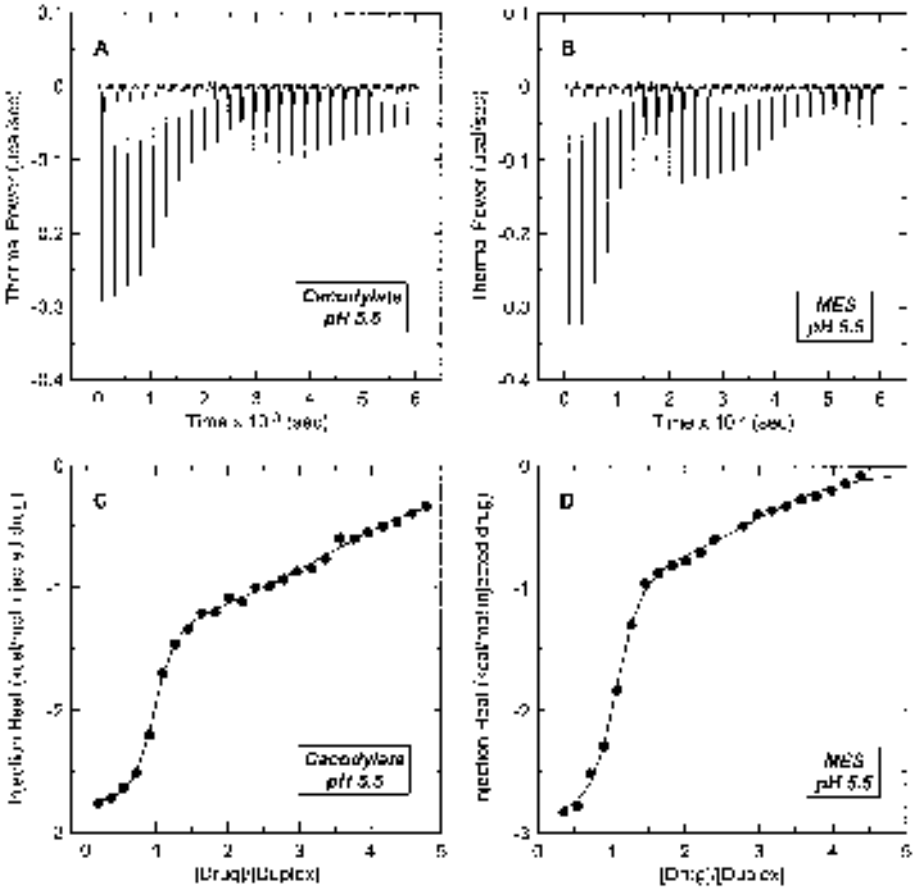

FIGURE 3 ITC profiles at 25°C for the titration of paromomycin sulfate into a solution of the A site RNA oligonucleotide at pH 5.5 in cacodylate (A, C) and MES (B, D) buffer. Each heat burst curve in panels A and B is the result of a 10 μL injection of 250 μM drug. The RNA concentration was 10 μM in strand, with each experimental solution containing 10 mM buffer, 0.1 mM EDTA, and sufficient NaCl to bring the total Na^+ concentration to 150 mM. The corrected injection heats shown in panels C and D were derived by integration of the corresponding heat burst curves shown in panels A and B, followed by subtraction of the corresponding dilution heats derived from control titrations of drug into buffer alone. The data points in panels C and D reflect the corrected experimental injection heats, while the solid lines reflect the calculated fits of the data. Data were taken from Kaul et al.[28]

opropane sulfonic acid, or TAPS (B and D) buffers at pH 9.0. A comparison of panels A and C with panels B and D reveals that the magnitude of the exothermic signal is substantially greater in bicine (ΔH_{ion} = +6.47 kcal/mol) than in TAPS (ΔH_{ion} = +9.92 kcal/mol). This observation is indicative of binding-linked proton uptake and is therefore consistent with binding-linked drug protonation.

Table II summarizes the observed enthalpies (ΔH_{obs}) derived from the ITC experiments shown in Figure 4, as well from corresponding experiments with neomycin and lividomycin sulfate conducted at pH 9.0 and 8.8, respectively. In addition, Table II also includes the values of ΔH_{int} and Δn, as calculated by solution of Eqs. (1a) and (1b). Inspection of these data reveals Δn values of 3.25 and 3.80 for paromomycin and neomycin sulfate at pH 9.0 and 3.25 for lividomycin sulfate at pH 8.8. Note that these values of Δn reflect contributions from all the drug amino groups whose protonation is linked to RNA complexation. In fact, the number of drug amino groups involved in RNA binding-linked proton uptake reactions at a given pH (the identities of which are defined below) can exceed the magnitude of the observed Δn at that pH.

A comparison of the Δn values listed in Table II with the protonation states of the drugs predicted by our NMR-derived pK_a values allows us to identify the specific drug amino groups whose protonation is linked to complexation with the host RNA. These

Table I ITC-Derived Binding Profiles at pH 5.5 for the Complexation of Paromomycin Sulfate with the A Site Model RNA Oligonucleotide at 25°C and a Na^+ Concentration of 150 m*M*[a]

Buffer	K_a[b] (M^{-1})	ΔH_{obs}[b] (kcal/mol)	N[b]
Cacodylate	$(3.7 \pm 0.7) \times 10^7$	-2.8 ± 0.1	0.9 ± 0.1
MES	$(3.8 \pm 1.3) \times 10^7$	-2.9 ± 0.1	1.0 ± 0.1

[a]Buffer solutions contained either 10 m*M* sodium cacodylate or 10 m*M* MES, 0.1 m*M* EDTA, and sufficient NaCl to bring the total Na^+ concentration to 150 m*M*.

[b]Values for the association constant (K_a), the observed binding enthalpy (ΔH_{obs}), and the binding stoichiometry (N) are derived from fits of the ITC profiles shown in Figure 3, with the indicated uncertainties reflecting the standard deviations of the experimental data from the fitted curves (depicted as solid lines in Figures 3C and D). Data are taken from Kaul et al.[28]

determinations reveal that the binding of lividomycin to the host RNA is coupled to the protonation of all five of its amino groups, with the RNA binding of paromomycin and neomycin being linked to the protonation of four and at least five amino groups, respectively. For paromomycin, the protonation reactions involve the 1-, 3-, 2′-, and 2‴-amino groups, while, for neomycin, the binding-linked protonation reactions involve at least the 1-, 3-, 2′-, 6′-, and 2‴-amino groups. In other words, these amino groups must be in their fully protonated NH_3^+ states when the drugs are bound to the host RNA. Note that this requirement is not evident in the previously reported NMR-derived and crystal structures of paromomycin in complex with various A site model RNA oligomers. Significantly, in these structures, the drug amino groups are in their deprotonated NH_2 states. Our results clearly identify drug protonation reactions as important thermodynamic participants in the specific binding of 2-DOS aminoglycosides to the A site of 16 S rRNA.

Estimation of the Average Heat of Protonation of Aminoglycoside Amino Groups

Inspection of the data in Table II reveals ΔH_{int} values of −37.8, −43.8, and −39.7 kcal/mol for the RNA binding of paromomycin, neomycin, and lividomycin, respectively. Although these ΔH_{int} values are independent of buffer ionization effects, they include contributions from *both* intrinsic drug–RNA interactions as well as binding-linked protonation reactions. Recall that the RNA binding of the three drugs at pH 5.5 is independent of drug protonation effects. In other words, the observed binding enthalpies (ΔH_{obs}) of the drugs at pH 5.5 do not include contributions from binding-linked protonation reactions. Thus, the enthalpic contributions from such protonation reactions ($\Delta H_{p\text{-}cont}$) to the values of ΔH_{int} listed in Table II can be determined from the difference between the values of ΔH_{obs} at pH 5.5 and the corresponding values of ΔH_{int} at the higher pH value. These calculations yield $\Delta H_{p\text{-}cont}$ values of −34.9, −39.6, and −34.0 kcal/mol for the binding of paromomycin (at pH 9.0), neomycin (at pH 9.0), and lividomycin (at pH 8.8), respectively. These values of $\Delta H_{p\text{-}cont}$ allow one to determine the *average* heats of protonation (ΔH_{prot}) of the drug amino groups whose protonation is linked to RNA complexation using the following relationship:

$$\Delta H_{prot} = \frac{\Delta H_{p-cont}}{\Delta n} \quad (2)$$

Solution of Eq. (2) yields ΔH_{prot} values of −10.7, −10.4, and −10.5 kcal/mol for paromomycin, neomycin, and lividomycin, respectively. These protonation heats are in excellent agreement with those previously reported[37] for the α-amino groups of amino acids, whose heats of protonation typically range from −9.2 to −10.9 kcal/mol, as well as for 2-amino- and 3-aminoglucose, whose heats of protonation are −10.2 and −10.1 kcal/mol, respectively.

THERMODYNAMICS OF AMINOGLYCOSIDE–rRNA RECOGNITION

Free Energy, Enthalpy, and Entropy of Complex Formation

We used ITC to characterize the binding of neomycin, paromomycin, lividomycin, and ribostamycin to the A site model oligonucleotide at pH 5.5 and a Na^+ concentration of 150 m*M*. By conducting such comparative studies at pH 5.5 (a pH at which the drugs are fully protonated), one can determine the impact of specific alterations in drug structure on the thermodynamics of RNA binding, *in the absence of contributions from drug protonation effects*. The thermodynamic binding profiles that resulted from our ITC studies are summarized in Table III. Inspection of the data in Table III reveals several significant features. Note that the potential role of hydration effects in the thermodynamics of aminoglycoside–RNA complexation is not included in our discussion of these fea-

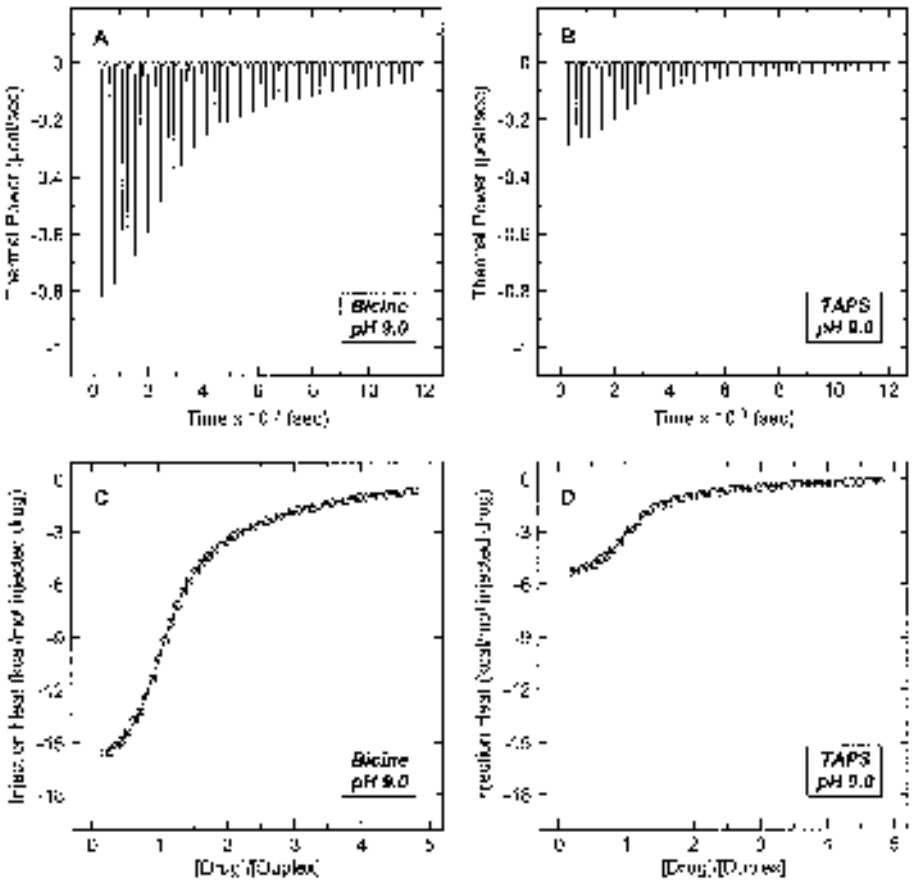

FIGURE 4 ITC profiles at 25°C for the titration of paromomycin sulfate into a solution of the A site RNA oligonucleotide at pH 9.0 in bicine (A, C) and TAPS (B, D) buffer. Each heat burst curve in panels A and B is the result of a 5 μL injection of 250 μM drug. The RNA concentration was 10 μM in strand, with each experimental solution containing 10 mM buffer, 0.1 mM EDTA, and sufficient NaCl to bring the total Na^+ concentration to 11 mM. The corrected injection heats shown in panels C and D were derived by integration of the corresponding heat burst curves shown in panels A and B, followed by subtraction of the corresponding dilution heats derived from control titrations of drug into buffer alone. The data points in panels C and D reflect the corrected experimental injection heats, while the solid lines reflect the calculated fits of the data. Data were taken from Kaul et al.[28]

tures, as it will be discussed separately in a later section.

Neomycin vs Paromomycin: 6′-NH_3^+ vs 6′-OH. Neomycin binds to the host RNA with a 1.2 kcal/mol higher affinity (7-fold in K_a) than paromomycin, an enhanced affinity similar in magnitude to those recently reported based on computational[38] and surface plasmon resonance studies.[39,40] This enhanced binding affinity of neomycin relative to that of paromomycin is the result of a more favorable (exothermic) binding enthalpy, with the entropic contributions to the RNA binding of both drugs being essentially identical. Recall that neomycin and paromomycin differ with respect to the substituent at the 6′ position, with this functionality being a hydroxyl group in paromomycin and an amino group in neomycin (see Figure 1). Thus, the presence of a 6′-amino vs a 6′-hydroxyl group results in an enthalpically driven enhancement in affinity. The molecular basis for this enthalpy-driven enhanced affinity may reflect contributions from a number of different potential sources, including differential hydrogen bonding and van der Waals interactions (which are typically manifested enthalpically). To evaluate this possibility, we conducted a series of computational studies using the NMR-derived structure of paromomycin in complex with the A-site model oligomer as a starting point.

Table II Number of Protons Linked to the Binding of Paromomycin, Neomycin, and Lividomycin Sulfate to the A Site Model RNA Oligonucleotide at pH 8.8 or 9.0 and a Na^+ Concentration of 11 m*M*[a]

Buffer (10 m*M*)	pH	ΔH_{ion}[b] (kcal/mol)	ΔH_{obs}[c] (kcal/mol)	ΔH_{int}[c] (kcal/mol)	Δn[c] (per drug)
			Paromomycin sulfate		
Bicine	9.0	+6.47	−16.8 ± 0.1	−37.8 ± 0.5	3.25 ± 0.06
TAPS	9.0	+9.92	−5.6 ± 0.1	−37.8 ± 0.5	3.25 ± 0.06
			Neomycin sulfate		
Bicine	9.0	+6.47	−19.2 ± 0.1	−43.8 ± 0.5	3.80 ± 0.06
TAPS	9.0	+9.92	−6.1 ± 0.1	−43.8 ± 0.5	3.80 ± 0.06
			Lividomycin sulfate		
Bicine	8.8	+6.47	−18.7 ± 0.1	−39.7 ± 0.5	3.25 ± 0.06
TAPS	8.8	+9.92	−7.5 ± 0.1	−39.7 ± 0.5	3.25 ± 0.06

[a]Buffer solutions contained either 10 m*M* bicine or 10 m*M* TAPS, 0.1 m*M* EDTA, and sufficient NaCl to bring the total Na^+ concentration to 11 m*M*. Data were taken from Kaul et al.[28]

[b]Ionization heats (ΔH_{ion}) at 25°C for the indicated buffers were taken from Fukada et al.[75] and Fukada and Takahashi (1987, unpublished results).

[c]The number of binding-linked protons (Δn) and intrinsic binding enthalpies (ΔH_{int}) at 25°C were calculated using Eqs. (1a) and (1b), as well as the corresponding experimentally observed binding enthalpies (ΔH_{obs}).

Specifically, we converted the amino groups of the paromomycin molecule in this complex to their protonated NH_3^+ states and then conducted a 1 ns molecular dynamics simulation on the resulting drug–RNA complex in which aqueous solvent was incorporated explicitly. In addition, we conducted a similar molecular dynamics simulation on the corresponding neomycin–RNA complex, following conversion the 6′-OH group of paromomycin to a NH_3^+ group. The lowest energy conformations of the paromomycin–RNA and neomycin–RNA complexes to emerge from these molecular dynamics simulations are shown in Figures 5 and 6, respectively. Note that neomycin forms three more direct hydrogen-bonding contacts with the host RNA than paromomycin (11 vs 8). These three additional hydrogen bonds may account, at least in part, for the enhanced affinity of neomycin for the RNA relative to paromomycin.

Neomycin vs Ribostamycin: Presence vs Absence of Ring IV. Neomycin binds to the host RNA with a 3.8 kcal/mol higher affinity (619-fold in K_a) than ribostamycin. Recall that ribostamycin differs from neomycin in that it lacks ring IV (see Figure 1). Thus, the presence of ring IV contributes substantially to affinity for the A site. Note that the enhanced affinity of neomycin for the A site relative to ribostamycin is 50% enthalpic and 50% entropic in origin. The reduced binding enthalpy of ribostamycin relative to neomycin may reflect diminished contacts with the host RNA by virtue of the ab-

Table III Thermodynamic Profiles at pH 5.5 for the Binding of 4,5-Disubstituted 2-DOS Aminoglycosides to the A Site Model RNA Oligonucleotide at 25°C and a Na^+ Concentration of 150 m*M*[a]

Drug	ΔH[b] (kcal/mol)	$T\Delta S$[c] (kcal/mol)	ΔG @ 25°C[c] (kcal/mol)	K_a @ 25°C[b] (M^{-1})
Paromomycin	−2.9 ± 0.1	+7.4 ± 0.2	−10.3 ± 0.1	$(3.7 \pm 0.7) \times 10^7$
Neomycin	−4.2 ± 0.1	+7.3 ± 0.2	−11.5 ± 0.1	$(2.6 \pm 0.7) \times 10^8$
Lividomycin	−5.7 ± 0.1	+4.8 ± 0.2	−10.5 ± 0.1	$(5.1 \pm 1.3) \times 10^7$
Ribostamycin	−2.3 ± 0.2	+5.4 ± 0.4	−7.7 ± 0.2	$(4.2 \pm 2.1) \times 10^5$

[a]Buffer solutions contained 10 m*M* sodium cacodylate, 0.1 m*M* EDTA, and sufficient NaCl to bring the total Na^+ concentration to 150 m*M*.

[b]Values of ΔH were derived from fits of ITC data, with the indicated uncertainties reflecting the standard deviations of the experimental data from the fitted curves. Values of K_a for paromomycin, lividomycin, and ribostamycin were also derived from fits of the corresponding ITC profiles, while the K_a for neomycin was derived using the ΔT_m-based approach described in the text.

[c]Values of $T\Delta S$ were determined using the standard relationship $T\Delta S = \Delta H - \Delta G$, while the values of ΔG were determined using the standard relationship $\Delta G = -RT\ln K$.

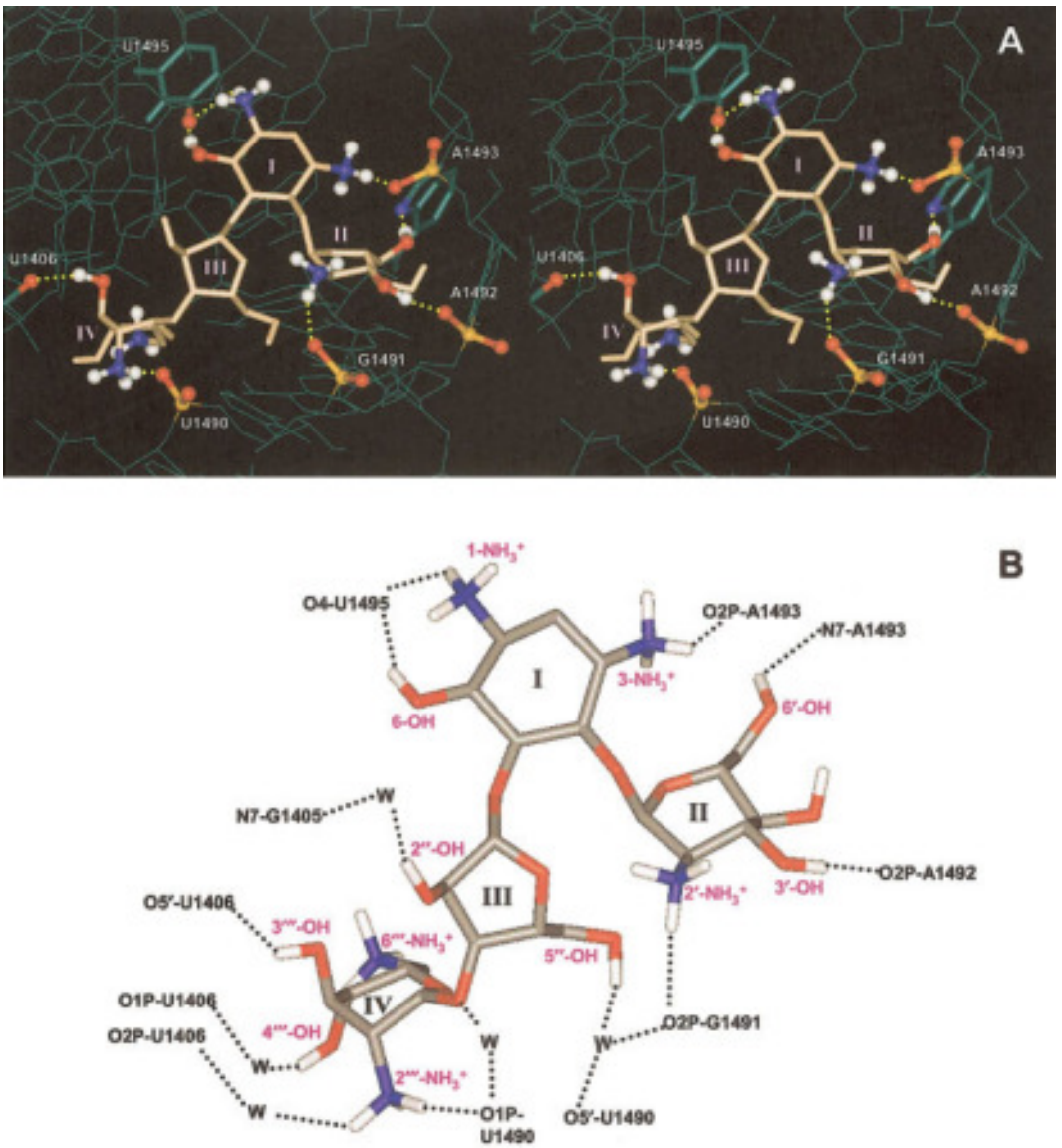

FIGURE 5 (A) Stereo view looking into the major groove of the fully protonated form of paromomycin in complex with the A site model RNA oligonucleotide. This structure represents the lowest energy conformation to emerge from computational studies conducted as described previously.[28] The drug is depicted in tan, while the RNA is depicted in green. The amino and hydroxyl groups of the drug that form direct hydrogen bonds with the host RNA are depicted as balls and sticks in standard CPK colors (nitrogen in blue, oxygen in red, and hydrogen in white). The hydrogen bonds are depicted as dotted yellow lines. The hydrogen bond accepting groups on the RNA (the phosphate groups of U1490, G1491, A1492, and A1493; the 4-carbonyl group of U1495; and the O5′ atom of U1406) are depicted as balls and sticks in standard CPK colors (phosphorus in orange). (B) Schematic representation of the direct and water (W)-mediated hydrogen bonds between the drug and the host RNA. In this representation, the color scheme for the drug atoms is as follows: Oxygen in red, nitrogen in blue, carbon in gray, and hydrogen in white.

sence of ring IV. In this regard, our computational studies discussed above reveal that ring IV of neomycin forms three direct and four water-mediated hydrogen bonding contacts with the target RNA (see Figure 6). Such contacts would be absent in the ribostamycin–RNA complex. The reduced binding entropy of ribostamycin relative to neomycin may reflect, at least in part, a diminished extent of binding-induced counterion release. Recall that our buffer-dependent ITC studies reveal that the 2″′-amino group on ring IV of neomycin must be protonated (charged) when the drug is bound to the target RNA. Furthermore, the computational studies

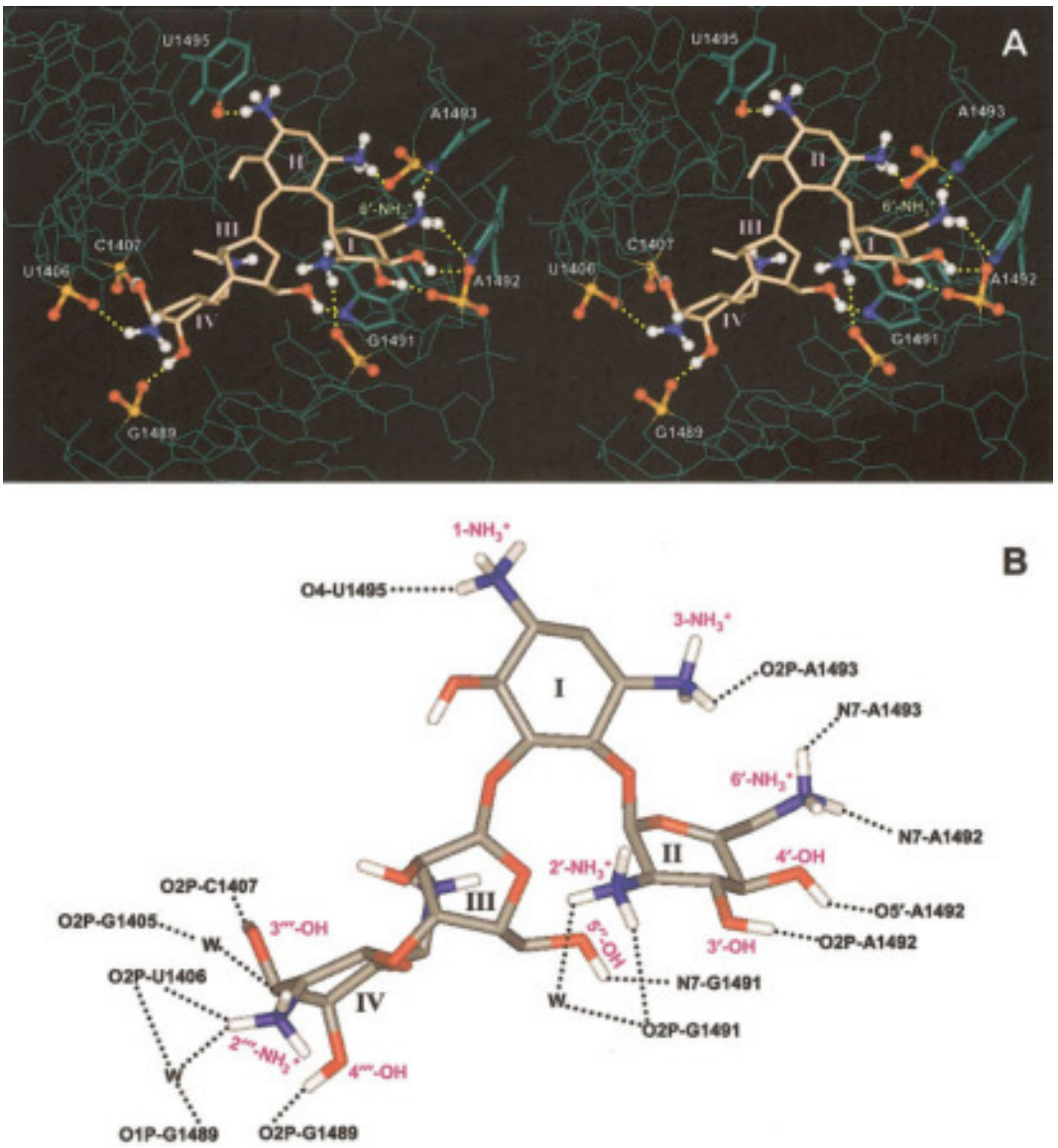

FIGURE 6 (A) Stereo view looking into the major groove of the fully protonated form of neomycin in complex with the A site model RNA oligonucleotide. This structure represents the lowest energy conformation to emerge from computational studies conducted as described previously.[28] The 6′-NH_3^+ group of the drug, which differs from the 6′-OH group present in paromomycin, is highlighted with a green label. In this complex, the hydrogen bond accepting groups on the RNA are as follows: The phosphate groups of U1406, C1407, G1489, G1491, and A1492, the 4-carbonyl group of U1495, the N7 atoms of G1491, A1492, and A1493, and the O5′ atom of A1492. (B) Schematic representation of the direct and water (W)-mediated hydrogen bonds between the drug and the host RNA. The color scheme for the drug is the same as described in the legend to Figure 5B.

discussed above reveal that this charged amino group makes electrostatic contact with the phosphate group of U1406. Such electrostatic contacts are typically associated with favorable entropies, since they are accompanied by counterion release. Any counterion release induced by the electrostatic interaction between the 2‴-amino group of neomycin and the phosphate group of U1406 would not occur in the RNA complex with ribostamycin, which lacks ring IV.

Paromomycin vs Lividomycin: Presence vs Absence of Ring V (a Mannopyranose Ring) and a 3′-OH Functionality. Lividomycin binds to the target RNA with a 2.8 kcal/mol more favorable enthalpy than

paromomycin. However, this gain in binding enthalpy is almost completely offset by a corresponding loss of 2.6 kcal/mol in the entropic contribution to binding, thereby yielding virtually identical binding free energies and constants for the two drugs (the differences being within the experimental uncertainty). In other words, the thermodynamic driving forces that dictate the similar binding affinities of the two drugs differ markedly, with the binding of paromomycin being primarily (72%) entropy driven and the binding of lividomycin being more (54%) enthalpy driven. Recall that the structures of lividomycin and paromomycin differ in two ways (see Figure 1): (a) Paromomycin contains a 3′-OH group, which lividomycin lacks. (b) Lividomycin has a mannopyranose moiety (a fifth ring) tethered to the 4‴ position in place of the 4‴-OH group that is present in paromomycin. Molecular dynamics studies on the paromomycin–RNA and lividomycin–RNA complexes reveal that the 3′-OH group of paromomycin makes hydrogen bonding contact with the O2 atom of the A1492 phosphate group (see Figure 5), while all four hydroxyl groups of the mannopyranose ring (ring V) of lividomycin form direct and/or water-mediated hydrogen bonds with the target RNA (not shown). It is likely that the enhanced binding enthalpy of lividomycin relative to paromomycin reflects, at least in part, the latter contacts involving ring V of lividomycin, which more than compensate the loss of the contact involving the 3′-OH group of paromomycin. The potential molecular origins of the reduced binding entropy of lividomycin relative to paromomycin are more difficult to address. Two obvious potential explanations are reduced extents counterion and water release upon the binding of lividomycin relative to paromomycin. However, our salt-dependent and osmolyte-dependent binding studies discussed in later sections indicate that paromomycin and lividomycin do not differ significantly with respect to these two binding behaviors. An alternative explanation for the reduced binding entropy of lividomycin relative to paromomycin may be that the two drug–RNA complexes have differential configurational entropies.

Heat Capacity Change Associated with Complex Formation

The heat capacity change (ΔC_p) associated with an aminoglycoside–RNA interaction can be determined from the temperature dependence of the observed binding enthalpy using the standard relationship:

$$\Delta C_p = \frac{\partial \Delta H_{obs}}{\partial T} \tag{3}$$

In this connection, we conducted additional ITC experiments to those described in the previous section, which were all conducted at 25°C, at two other temperatures, 35 and 45°C. Figure 7 shows representative ITC profiles for the RNA binding of paromomycin at 25°C (A), 35°C (B), and 45°C (C). Note that the observed binding enthalpy becomes increasingly exothermic with increasing temperature. Table IV summarizes the ΔH_{obs} values derived from the ITC profiles shown in Figure 7, as well as from corresponding ITC studies with neomycin and lividomycin. Inspection of the data in Table IV reveals that, like paromomycin, the observed binding enthalpies of neomycin and lividomycin also become increasingly exothermic with increasing temperature. Figure 8 graphically portrays the data in Table IV in the form of ΔH_{obs} vs temperature plots. The data points in these plots were fit by linear regression, with the slopes of the resulting lines yielding estimates of ΔC_p for the RNA binding of the three drugs. This analysis yielded ΔC_p values of -210, -290, and -180 cal/mol · K for the binding of paromomycin, neomycin, and lividomycin, respectively (Table IV). The magnitude and sign of these ΔC_p values fall within the range of -100 to -550 cal/mol · K that is typically observed for both ligand–nucleic acid as well as ligand–protein interactions.[41–45]

Reductions in solvent accessible surface are thought to have an impact on the value of ΔC_p, with the burial of nonpolar surfaces causing ΔC_p values to be more negative and the burial of polar surfaces causing ΔC_p values to be more positive.[42,44–47] Thus, it is tempting to ascribe the negative ΔC_p values we observe accompanying aminoglycoside–RNA complexation to binding-induced reductions in nonpolar solvent accessible surface. However, our osmotic stress studies described in a later section reveal little or no net change in hydration upon aminoglycoside–RNA complexation, an observation consistent with complex formation being accompanied by little or no net change in solvent-accessible surface. Hence, it is unlikely that our observed negative ΔC_p values reflect binding-induced alterations in solvent accessible surface. As detailed in the section below, electrostatic interactions play a role in stabilizing aminoglycoside–rRNA complexes. Electrostatic interactions can also have an impact on observed ΔC_p.[48] However, Sharp and co-workers have shown that this impact is positive in sign and small in magnitude (15–90 cal/mol · K).[48] Thus, our observed negative ΔC_p values are not the result of electrostatic interactions, although they are likely to include small positive contributions from such interactions. Another potential contributor to ΔC_p is binding-induced conformational change. In

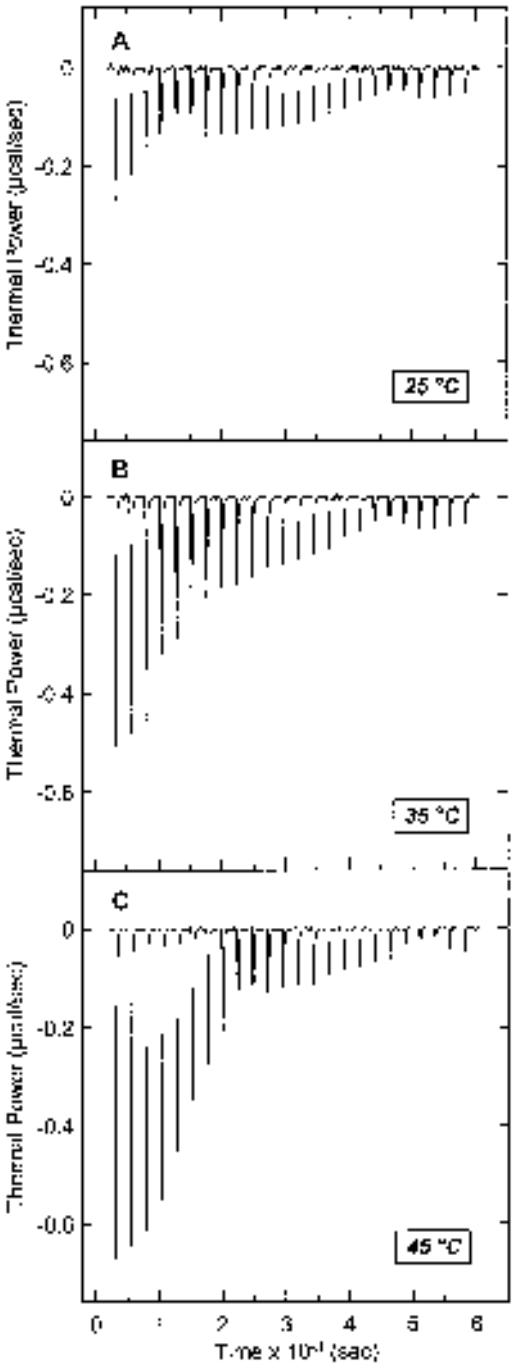

FIGURE 7 ITC profiles for the binding of paromomycin to the A site model RNA oligonucleotide at 25°C (A), 35°C (B), and 45°C (C). Each heat burst curve is the result of a 10 μL injection of 250 μM drug into a solution of RNA 10 μM in strand. The experimental solution conditions were 10 mM sodium cacodylate (pH 5.5), 0.1 mM EDTA, and sufficient NaCl to bring the total Na^+ concentration to 150 mM. The ITC experiments were conducted as described previously.[28]

this regard, structural studies[9,11,14,16,30] have shown that aminoglycoside binding to the rRNA A site induces a conformational change in the host RNA, the details of which are highlighted in the introduction. Furthermore, Eftink et al.[49] have demonstrated that binding-linked conformational changes can result in negative apparent heat capacity changes of the same magnitude as those reported here. We therefore suggest that our observed negative heat capacity changes reflect, at least in part, aminoglycoside-induced changes in the structure of target RNA.

SALT DEPENDENCE OF AMINOGLYCOSIDE–rRNA RECOGNITION

In order to determine the salt dependence of the aminoglycoside–RNA association constants at pH 5.5, we employed an approach that is predicated on the extent to which drug binding enhances the thermal stability (as measured by the drug-induced change in duplex melting temperature, ΔT_m) of the host RNA. Specifically, we measured the aminoglycoside-induced ΔT_m over a range of Na^+ concentrations to

Table IV Temperature Dependence of the Enthalpies and Corresponding Heat Capacity Changes for the Binding of Paromomycin, Neomycin, and Lividomycin Sulfate to the A Site Model RNA Oligonucleotide at pH 5.5[a]

Drug	Temperature (°C)	ΔH_{obs}[b] (kcal/mol)	ΔC_p[c] (cal/mol · K)
Paromomycin	25	−2.8 ± 0.1	
Paromomycin	35	−4.8 ± 0.1	−210 ± 10
Paromomycin	45	−7.0 ± 0.1	
Neomycin	25	−4.2 ± 0.1	
Neomycin	35	−7.0 ± 0.1	−290 ± 10
Neomycin	45	−10.0 ± 0.1	
Lividomycin	25	−5.7 ± 0.1	
Lividomycin	35	−7.3 ± 0.1	−180 ± 12
Lividomycin	45	−9.3 ± 0.1	

[a]Buffer solutions contained 10 mM sodium cacodylate, 0.1 mM EDTA, and sufficient NaCl to bring the total Na^+ concentration to either 150 mM (for paromomycin and lividomycin) or 200 mM (for neomycin).

[b]Values of ΔH_{obs} were derived from fits of ITC data, with the indicated uncertainties reflecting the standard deviations of the experimental data from the fitted curves.

[c]Heat capacity changes (ΔC_p) were derived from linear regression analyses of the plots shown in Figure 8, with the indicated uncertainties reflecting the standard deviations of the experimental data from the fitted lines.

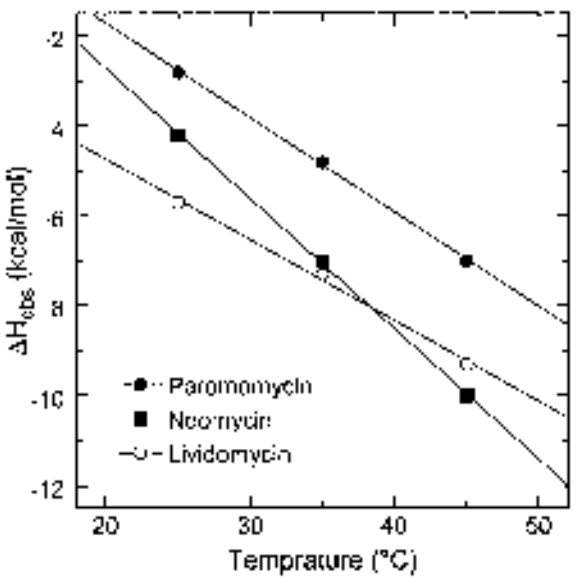

FIGURE 8 Temperature dependence of the observed enthalpies (ΔH_{obs}) for the binding of paromomycin (filled circles), neomycin (filled squares), and lividomycin (open circles) to the A-site model RNA oligonucleotide. The experimental data points (which were derived from ITC experiments conducted in cacodylate buffer at pH 5.5 and Na^+ concentration of 150 m*M*) were fit by linear regression, with the resulting fits depicted as solid lines.

estimate the apparent drug–RNA association constant at T_m (K_{Tm}) from the following expression[50]:

$$\frac{1}{T_{m0}} - \frac{1}{T_m} = \frac{NR}{\Delta H_{Dup}} \ln(1 + K_{T_m} L) \tag{4}$$

In this expression, T_{m0} and T_m are the melting temperatures of the drug-free and drug-bound duplex, respectively, N is the number of drug molecules bound per duplex, ΔH_{Dup} is the enthalpy change for the melting of the duplex in the absence of bound drug [a value we determined by differential scanning calorimetry (DSC) to be $+76.0 \pm 2.5$ kcal/mol], and L is the free drug concentration at T_m (which can be estimated by one half the total drug concentration). We then extrapolated this binding constant at T_m to a reference temperature of 25 °C ($K_{25}^{T_m}$) using the following relationship[51]:

$$K_T = \frac{K_{T_m}}{e^{(-\Delta H_T/R)\,[(1/T_m)-(1/T)]} e^{(-\Delta C_P T/R)\,[(1/T_m)-(1/T)]} (T_m/T)^{\Delta C_P/R}} \tag{5}$$

The resulting $K_{25}^{T_m}$ values of paromomycin, neomycin, and lividomycin are listed in Table V. Note that, for each drug, $K_{25}^{T_m}$ decreases with increasing Na^+ concentration. This observation indicates that electrostatic interactions play an important role in the binding of the drugs to the host RNA duplex. Record and co-workers have derived the following relationship[52]:

$$\left(\frac{\partial \log K_{25}^{Tm}}{\partial \log[Na^+]}\right) = -Z\varphi \tag{6}$$

In this relationship, Z denotes the apparent charge on the bound ligand and φ is the fraction of Na^+ bound per RNA phosphate. The value of φ for the A-form poly(rA) · poly(rU) duplex is 0.89, while that for single-stranded poly(rA) is 0.78.[52] It is likely that the φ value for the internal loop region of the A site is intermediate between these two values. Equation (6)

Table V Salt Dependence of the ΔT_m-Derived Association Constants at 25°C for the Complexation of Paromomycin, Neomycin, and Lividomycin Sulfate with the A Site Model RNA Oligonucleotide at pH 5.5[a]

$[Na^+]$ (m*M*)	T_{m0}[b] (°C)	T_m[b] (°C)	K_{25}^{Tm}[c] (M^{-1})
		Paromomycin	
109	70.9	78.0	$(6.8 \pm 1.7) \times 10^7$
129	71.8	77.4	$(3.8 \pm 0.9) \times 10^7$
150	72.4	77.0	$(2.5 \pm 0.6) \times 10^7$
174	73.3	76.6	$(1.4 \pm 0.3) \times 10^7$
200	73.6	76.0	$(8.4 \pm 2.2) \times 10^6$
		Neomycin	
109	70.9	81.7	$(7.2 \pm 2.1) \times 10^8$
129	71.8	81.4	$(4.7 \pm 1.3) \times 10^8$
150	72.4	80.5	$(2.6 \pm 0.7) \times 10^8$
174	73.3	79.6	$(1.3 \pm 0.3) \times 10^8$
200	73.6	79.2	$(9.9 \pm 2.4) \times 10^7$
		Lividomycin	
109	70.9	77.8	$(1.1 \pm 0.3) \times 10^8$
129	71.8	77.6	$(7.0 \pm 2.0) \times 10^7$
150	72.4	77.0	$(4.2 \pm 1.2) \times 10^7$
174	73.3	76.6	$(2.3 \pm 0.7) \times 10^7$
200	73.6	76.5	$(1.9 \pm 0.5) \times 10^7$

[a]Buffer solutions contained 10 m*M* sodium cacodylate, 0.1 m*M* EDTA, and sufficient NaCl to bring the total Na^+ concentration to the value indicated in column 1.

[b]T_m values were derived from uv melting profiles of the A-site model oligonucleotide in the absence (T_{m0}) and presence of drug (at a total drug to RNA ratio of 1.0), with an uncertainty in the data of ±0.1°C. The UV melting experiments were conducted as previously described.[35]

[c]Association constants at 25°C (K_{25}^{Tm}) were determined as described in the text, with the indicated uncertainties reflecting the maximum errors as propagated through Eqs. (4) and (5).

postulates that an estimate for the minimum number of drug NH_3^+ groups that participate in electrostatic interactions ($Z\varphi$) with the host RNA can be derived from plots of $\log(K_{25}^{T_m})$ vs $\log([Na^+])$. Such plots for the data listed in Table V are shown in Figure 9. Note the linear dependencies of the data for all three drugs, which upon linear regression analyses, yield slopes of -3.4 ± 0.1 for paromomycin, -3.5 ± 0.2 for neomycin, and -3.1 ± 0.2 for lividomycin. These values of $-Z\varphi$ indicate that at least four NH_3^+ groups on each drug participate in electrostatic interactions with the host RNA, an observation consistent with our pH-dependent ITC and NMR studies discussed above, which revealed the RNA binding of paromomycin, lividomycin, and neomycin to be coupled to the protonation of four, five, and at least five amino groups, respectively. In the aggregate, these data suggest that electrostatic interactions provide the driving force for most if not all the observed RNA binding-linked drug protonation reactions.

Our structural models of the aminoglycoside–RNA complexes provide insight into the nature of the electrostatic contacts that drive the protonation reactions. Using the paromomycin–RNA complex as an illustrative example, Figure 5 reveals that the 3-, 2′-, and 2‴-amino groups of the drug make hydrogen-bonding contacts with the phosphate groups of A1493, G1491,

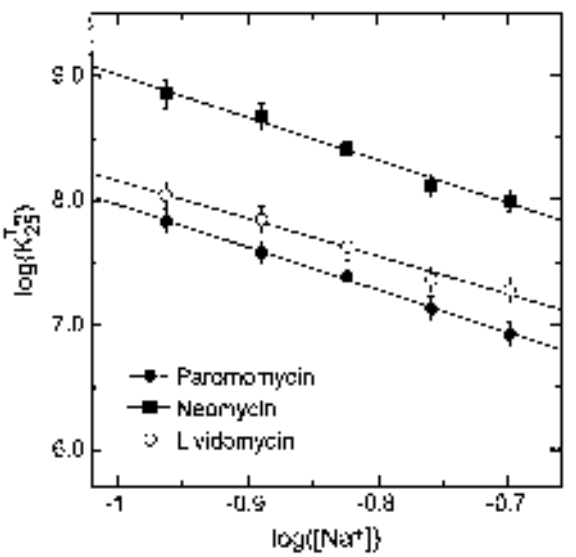

FIGURE 9 Salt dependence of the ΔT_m-derived association constants at 25°C ($K_{25}^{T_m}$) for the binding of paromomycin (filled circles), neomycin (filled squares), and lividomycin (open circles) to the A site RNA oligonucleotide at pH 5.5. Plots of $\log(K_{25}^{T_m})$ vs $\log([Na^+])$ for the three drugs were derived from the data in Table V. The experimental data points were fit by linear regression, with the resulting fits depicted as solid lines.

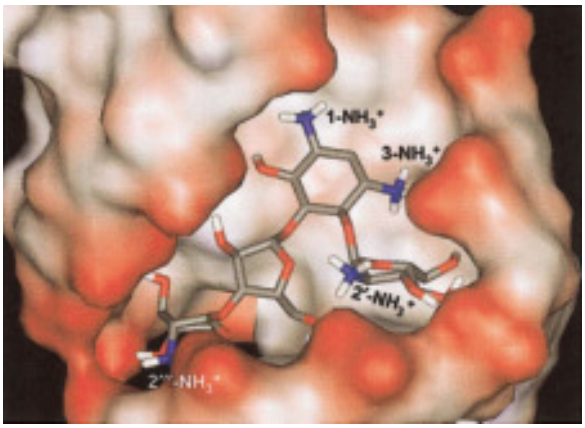

FIGURE 10 Another representation of the same paromomycin–RNA complex shown in Figure 5 in which the RNA is depicted in its solvent accessible surface (water probe radius = 1.4 Å). The surface of the RNA is colored according to its electrostatic potential, with red being negative, white being neutral, and blue being positive. The drug is depicted according to the same coloring scheme as described in the legend to Figure 5B. The four drug amino groups whose protonation is coupled to RNA binding are indicated.

and U1490, respectively. The close proximity of these cationic amino and anionic phosphate groups is also indicative of favorable electrostatic interactions between the charged functionalities. These favorable electrostatic contacts are highlighted in Figure 10, which presents a view of the drug–RNA complex in which the RNA is depicted in its solvent-accessible surface and colored according to its electrostatic potential. It is likely that these electrostatic contacts provide the driving force for the observed RNA binding-linked protonation of the 3-, 2′-, and 2‴-amino groups noted above in an earlier section. In contrast to these three amino groups, the 1-amino group of paromomycin, whose protonation is also linked to RNA complexation, does not form contacts with any phosphate functionalities on the RNA. Instead, it is directed toward the floor of the major groove, forming a hydrogen bond with the 4-carbonyl group of U1495 (see Figure 5). Note that the region of the major groove surrounding the 1-NH_3^+ group is an area of electronegative potential (see Figure 10) formed by the 4-carbonyl groups of U1406 and U1495, as well as the 6-carbonyl group of G1494. Thus, the RNA binding-linked protonation of the 1-NH_3^+ group may be driven by favorable electrostatic interactions between this cationic functionality of the drug and the electronegative region of the major groove toward which it is directed.

In addition to electrostatic contacts, hydrogen-bonding interactions between drug amino groups and

Table VI Osmolyte Dependence of the ITC-Derived Association Constants at 35°C for the Binding of Paromomycin and Lividomycin Sulfate to the A Site Model RNA Oligonucleotide at pH 5.5 and a Na^+ Concentration of 150 m*M*[a]

Drug	Osmolyte	Osmolality (Osm)	K_a[b] (M^{-1})	$K_{a\text{-}Osm}$[b] (M^{-1})
Paromomycin	None	0	$(1.7 \pm 0.3) \times 10^7$	—
Paromomycin	Sucrose	2.3	—	$(1.0 \pm 0.2) \times 10^7$
Paromomycin	Tri(ethylene glycol)	4.6	—	$(1.2 \pm 0.2) \times 10^7$
Lividomycin	None	0	$(1.1 \pm 0.1) \times 10^7$	—
Lividomycin	Sucrose	2.3	—	$(1.2 \pm 0.2) \times 10^7$
Lividomycin	Tri(ethylene glycol)	4.6	—	$(1.1 \pm 0.2) \times 10^7$

[a]Buffer solutions contained 10 m*M* sodium cacodylate, 0.1 m*M* EDTA, and sufficient NaCl to bring the total Na^+ concentration to 150 m*M*. Experimental RNA and drug solutions for use in osmotic stress experiments were prepared as follows: (a) Appropriate aliquots of buffer and drug or buffer and RNA were combined and lyophilized to dryness. (b) The lyophilized pellets then were resuspended in the appropriate volume of an osmolyte solution [sucrose or tri(ethylene glycol)] at the desired osmolality. The osmolalities of the experimental solutions were measured using a Fiske Model 2400 Multi-Sample Osmometer. Control UV melting experiments were conducted (as previously described[35]) to ensure that the RNA remained in its folded duplex form in the presence of the osmolytes. The presence of the osmolytes decreased the T_m of the RNA. However, at the concentrations of osmolyte used here, the T_m of the RNA remained well above the temperature used in our binding studies.

[b]Association constants in the presence ($K_{a\text{-}Osm}$) and absence (K_a) of osmolyte were derived from fits of ITC data, with the indicated uncertainties reflecting the standard deviations of the experimental data from the fitted curves. The ITC experiments using the osmolyte-containing solutions were conducted at 35°C as previously described.[28]

the RNA bases may also play a role in driving certain observed protonation reactions. A potential example of this behavior suggested by our computational studies involves the 6′-amino group of neomycin. Recall that protonation of the 6′-amino group is coupled to formation of the neomycin–RNA complex. In other words, the 6′-amino group of neomycin must be in its protonated state when the drug is bound to the host RNA. Despite this requirement, the $-Z\varphi$ value of neomycin is essentially identical to that of paromomycin, whose sole structural difference relative to neomycin is the presence of a 6′-hydroxyl group instead of an amino group (see Figure 1). Molecular dynamics studies of the neomycin–RNA complex reveal that the 6-NH_3^+ group of the drug makes hydrogen-bonding contact with the N7 atoms of both A1492 and A1493 (see Figure 6). Thus, the binding-linked protonation of the 6′-amino group of neomycin may be driven by hydrogen-bonding interactions with RNA bases rather than electrostatic interactions with electronegative regions of the RNA.

HYDRATION AND AMINOGLYCOSIDE–rRNA RECOGNITION

The osmotic stress method has been used extensively to evaluate the participation of water molecules in a wide variety of biochemical reactions.[53,54] One version of this method involves the addition of neutral solutes or cosolvents to solutions containing the macromolecules and the ligands being studied, thereby altering the water activity in the solution. We used this osmotic stress method to investigate the hydration changes that accompany the binding of paromomycin and lividomycin to the A-site model RNA oligonucleotide. In these studies, we evaluated the impact of two different osmolytes, sucrose and tri(ethylene glycol) (TEG), on the ITC-derived affinities of paromomycin and lividomycin for the host RNA at pH 5.5 and a Na^+ concentration of 150 m*M*. These two osmolytes have been used successfully to study water uptake or release in DNA duplex and triplex melting reactions,[55] in the interaction of *gal* repressor with DNA,[56] and in the interactions of intercalating ligands with DNA.[57] Table VI summarizes the drug–RNA association constants obtained in the presence ($K_{a\text{-}Osm}$) and absence (K_a) of osmolytes at the indicated osmolalities (Osm). Note that, for both drugs, the presence of either 2.3 Osm sucrose or 4.6 Osm TEG does not significantly alter affinity for the target RNA, with the difference between $K_{a\text{-}Osm}$ and K_a being essentially within the experimental uncertainty. These observations suggest that the RNA binding of paromomycin and lividomycin is accompanied by little or no net change in hydration. In other words, under the experimental conditions employed, we find no evidence for a net uptake or release of water upon complex formation. This result is somewhat surprising in light of recent crystallographic studies,[14,16] as

well as our computational studies, which reveal numerous water-mediated interactions in aminoglycoside–rRNA complexes. It is possible that such interactions make use of water molecules that preexist in the hydration shells of the free RNA and/or drugs, a concept that has been previously proposed by the Westhof group based on an analysis of the hydration patterns in the crystal structures of a multitude of nucleic acids as well as of protein–nucleic acid and drug–nucleic acid complexes.[58–60] In the aggregate, our osmotic stress studies suggest that water does not provide a major driving force in the binding of paromomycin and lividomycin to the A site of rRNA. The generality of this observation with regard to other aminoglycosides remains to be assessed.

PARSING THE FREE ENERGY CONTRIBUTIONS TO AMINOGLYCOSIDE–rRNA BINDING REACTIONS

The Chaires group has recently presented a conceptual model for parsing the observed free energies of drug–nucleic acid interactions into contributions from the various molecular processes that accompany complex formation.[43,45] This model, which assumes the additivity of free energy contributions, expresses the observed binding free energy (ΔG_{obs}) as the sum of contributions from at least five terms:

$$\Delta G_{obs} = \Delta G_{t+r} + \Delta G_{conf} + \Delta G_{hyd} + \Delta G_{pe} + \Delta G_{mol} \quad (7)$$

The five terms on the right-hand side of this expression are defined as follows: ΔG_{t+r} is the free energy cost resulting from the losses of translational and rotational degrees of freedom that accompany bimolecular complex formation. ΔG_{conf} is the free energy contribution from binding-induced conformational changes in both the nucleic acid and the drug. ΔG_{hyd} is the free energy change associated with the hydrophobic transfer of the drug from solution into its nucleic acid binding site. ΔG_{pe} is the polyelectrolyte contribution to the binding free energy that arises from the binding-induced release of condensed counterions from the nucleic acid. ΔG_{mol} is the free energy contribution from noncovalent interactions between the drug and the nucleic acid, which include hydrogen-bond formation and van der Waals interactions. We describe below how we have employed the model described by Eq. (7) to parse the observed free energy for the binding of paromomycin to the A-site model RNA oligonucleotide.

Entropic Cost of Bimolecular Complex Formation (ΔG_{t+r})

ΔG_{t+r} reflects the entropic penalty associated with bimolecular complex formation that results from a loss of translational and rotational degrees of freedom. Application of the Sakur–Tetrode equation,[61] describing the translational entropy of a monatomic ideal gas, has yielded a theoretical estimate of +15 kcal/mol for ΔG_{t+r}.[62,63] An essentially identical value of 14.9 ± 3.0 kcal/mol at 25 °C was derived empirically by the Record group,[47] based on consideration of specific instances of rigid body associations. We therefore use this value of ΔG_{t+r} in our parse of the paromomycin–RNA binding free energy. It should be noted that lower estimates of ΔG_{t+r} in the range of +6–10 kcal/mol also have been reported.[64,65] Thus, +15 kcal/mol may reflect an upper limit for the value of ΔG_{t+r}.

Estimation of ΔG_{conf} for Paromomycin–rRNA Complex Formation

As noted above, NMR and crystallographic studies of paromomycin in complex with both model rRNA oligonucleotides and the 30 S ribosomal subunit have revealed that the binding of the antibiotic causes a local conformational change in the A site of the RNA, which involves the displacement of A1492 and A1493 toward the minor groove.[9,11,14,16,30,33] This conformational change results in both bases becoming essentially destacked from the helix. Previously reported thermodynamic studies[66,67] of base-stacking interactions in riboadenylic acid polymers and oligomers provide us with a means of deriving an estimate for the free energy cost associated with the destacking of A1492 and A1493. These thermodynamic studies indicate that the disruption of an ApA stack is associated with a free energy cost of approximately +0.5 kcal/mol.[66,67] The destacking of A1492 and A1493 involves the disruption of the stack that exists in the drug-free RNA between A1492 and A1493 as well as the stack between A1493 and G1494. With the reasonable assumption that the free energy associated with an ApA stack is similar to that associated with an ApG stack, we estimate a value of +1 kcal/mol for ΔG_{conf}. A second binding-induced alteration in the structure of the host RNA revealed by the NMR studies cited above is a bend in the RNA helical axis.[9,11] Like the destacking of the two adenine residues, such a conformational change should also be

energetically costly.[68] However, it is difficult to derive a meaningful quantitative estimate for this free energy cost, since the thermodynamics of RNA bending are poorly understood. Instead, we note that our estimate of +1 kcal/mol for ΔG_{conf} should probably be considered a lower limit.

Hydrophobic Contributions (ΔG_{hyd}) to Paromomycin–rRNA Complex Formation

Record and co-workers have derived the following empirical formalism relating the free energy of hydrophobic transfer (ΔG_{hyd}) and the heat capacity change (ΔC_p) for a binding reaction:[47,69]

$$\Delta G_{hyd} = 80\ (\pm 10) \times \Delta C_p \qquad (8)$$

This formalism implies that ΔG_{hyd} can be determined in a straightforward and direct way by experimentally determining ΔC_p. Recall that our temperature-dependent ITC measurements yielded a ΔC_p value of −210 cal/mol · K for the RNA binding of paromomycin, which, in turn, would appear to imply a corresponding ΔG_{hyd} value of −16.8 kcal/mol. However, as discussed above, we believe that our observed ΔC_p reflects a binding-induced conformational change in the target RNA rather than binding-induced burial of hydrophobic surface. For this reason, we suggest a hydrophobic contribution to the binding free energy of essentially zero.

Polyelectrolyte Contributions (ΔG_{pe}) to Paromomycin–rRNA Complex Formation

Our salt-dependent binding studies described above yielded a $Z\varphi$ value of 3.4 for the RNA binding of paromomycin. This value of $Z\varphi$ allows us to determine the polyelectrolyte contribution to the observed binding free energy (ΔG_{pe}) using the following relationship[52]:

$$\Delta G_{pe} = Z\varphi RT \ln([Na^+]) \qquad (9)$$

Solution of Eq. (9) yields a ΔG_{pe} value of −3.8 kcal/mol for the A site RNA binding of paromomycin at 150 m*M* Na^+. Thus, while ΔG_{pe} is an important favorable contributor to the overall free energy of paromomycin–RNA complex formation, it is not sufficiently large in magnitude to overcome the unfavorable free energies associated with binding-induced conformational changes and the reduction in translational and rotational degrees of freedom that accompany complex formation ($\Delta G_{conf} + \Delta G_{t+r} = +16.0$ kcal/mol).

Contributions to Paromomycin–rRNA Complex Formation from Molecular Interactions (ΔG_{mol})

Determining the free energy contributions of noncovalent molecular interactions (e.g., hydrogen bonds and van der Waals contacts) formed upon drug–RNA complexation is one of the more challenging tasks that confronts us. Numerous such contacts have been described in the structures of the aminoglycoside–rRNA complexes reported to date.[9,14,16,33] In principle, it should be possible to sum up the free energies associated with each type of interaction using estimates for the thermodynamic parameters for each type of noncovalent bond. The problem with this type of approach is that there is no general consensus for the free energy contribution of each type of noncovalent interaction. Reported estimates for the thermodynamic parameters associated with various noncovalent interactions vary widely,[70,71] highlighting the lack of a general consensus. An alternative approach is to subtract the sum of the free energy contributions from entropic, conformational, hydrophobic, and polyelectrolyte effects ($\Delta G_{t+r} + \Delta G_{conf} + \Delta G_{hyd} + \Delta G_{pe}$) from the observed binding free energy (ΔG_{obs}), and then attribute the resulting free energy difference to all the remaining noncovalent interactions. The Chaires and Wilson groups have applied this approach to parse the free energy of a broad range of drug–DNA interactions, including both intercalative and minor groove-directed interactions.[42–44,72] Here, we use this approach to complete our parse of the paromomycin–RNA binding free energy observed at pH 5.5 and 150 m*M* Na^+. The resulting energetic contributions to the overall binding free energy are shown in Figure 11. The observed binding free energy (ΔG_{obs}) is −10.3 kcal/mol. This ΔG_{obs} is achieved because the unfavorable contributions resulting from the entropic cost of complex formation (ΔG_{t+r}) and binding-induced conformational changes (ΔG_{conf}) are overcome by favorable contributions from polyelectrolyte effects (ΔG_{pe}) and specific molecular interactions (ΔG_{mol}), with ΔG_{mol} providing the major favorable contribution (−22.5 kcal/mol) to binding free energy. This value of ΔG_{mol} is fully consistent with NMR,[9] crystallographic,[14] and computational (see Figure 5) studies on paromomycin–rRNA complexes, which reveal 8–13 direct and 11–12 water-mediated hydrogen bonds between the drug and the RNA. Recent studies by the Chaires and Wilson groups probing the DNA binding energetics of a broad range of

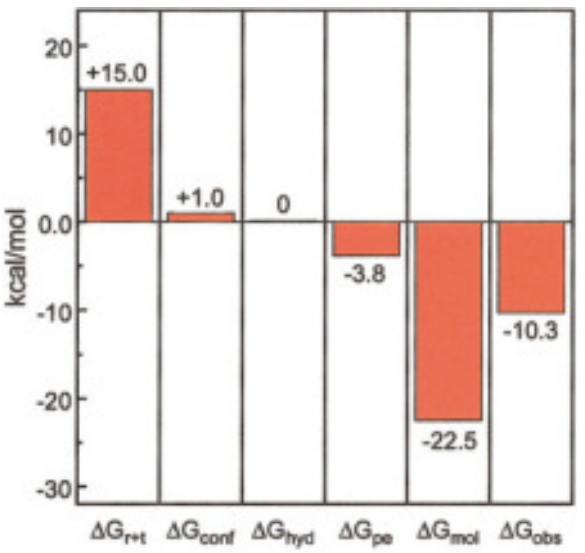

FIGURE 11 Parsing the free energy of paromomycin binding to the A-site model RNA oligonucleotide at pH 5.5 (i.e., in the absence of binding-induced drug protonation effects). The estimated contributions to the observed binding free energy (ΔG_{obs}) from the different sources discussed in the text are shown. For reasons discussed in the text, the free energy contribution from the hydrophobic transfer process (ΔG_{hyd}) is assumed to be 0. ΔG_{t+r} is the free energy contribution from changes in translational and rotational degrees of freedom upon bimolecular complex formation, ΔG_{conf} is the free energy contribution from binding-induced conformational changes, ΔG_{pe} is the polyelectrolyte contribution to the binding free energy, and ΔG_{mol} is the free energy contribution from the formation of specific noncovalent molecular interactions between the drug and host RNA.

intercalating and minor groove-directed ligands have demonstrated that hydrophobic effects (ΔG_{hyd}) provide major driving forces for complex formation.[42–44,72] In some cases, the contribution from ΔG_{mol} was substantially lower in magnitude than that from ΔG_{hyd}.[42,44] These observations are in marked contrast to those reported here for paromomycin–rRNA complex formation, which is 86% driven by drug–RNA contacts (ΔG_{mol}). This difference is likely due to the highly polar nature of paromomycin and aminoglycosides in general, a feature that distinguishes them from most DNA binding ligands, which typically contain more nonpolar atoms and fewer discrete charges than the aminoglycosides.

SUMMARY AND CONCLUDING REMARKS

Recent NMR and crystallographic studies have provided important structural information about aminoglycoside-rRNA interactions.[9,11,14–16,30,33] Correlation of this valuable structural information with the RNA binding affinities and specificities exhibited by the aminoglycosides requires detailed thermodynamic information to complement the existing structural database. The studies described in this article are intended to provide the requisite thermodynamic information.

We have previously demonstrated that the protonation state of the aminoglycoside is a critical factor in determining the affinity of the drug for its designated RNA target.[28,34,35] It is therefore important to understand the pH-dependent chemical properties of the aminoglycosides, as well as the nature of the relationship between these properties and the RNA binding affinity and specificity exhibited by the drugs. Such information would be difficult to obtain from structural studies alone. The pH- and buffer-dependent ITC studies described here have allowed us to determine the number of protons linked to the complexation of several aminoglycosides with an A-site model RNA oligomer at pH values >5.5. By comparing the number of RNA binding-linked protons to the protonation states of the drugs predicted by NMR-derived pK_a values, we have also identified the specific drug amino groups whose protonation is linked to complexation with the host RNA. We have used this information and the existing structural database to generate explicitly solvated structural models of several aminoglycoside–rRNA complexes in which the drugs are in the protonated and charged states dictated by our results. These models provide important insights into the noncovalent drug–RNA interactions (e.g., hydrogen bonds, van der Waals interactions, and electrostatic interactions) that drive the observed binding-linked protonation reactions and contribute to the stabilities of the drug–RNA complexes. In the aggregate, our pH- and buffer-dependent binding studies clearly identify drug protonation reactions as important thermodynamic participants in the binding of aminoglycosides to specific RNA targets. Such protonation reactions also have the potential of influencing the interactions of aminoglycosides with other macromolecular targets. In this connection, Fong and Berghuis[73] have recently reported crystal structures of both neomycin and kanamycin A in ternary complex with the aminoglycoside kinase APH(3′)-IIIa and ADP. Significantly, both complexes involve substantial interactions between negatively charged amino acid residues at the C-terminus of the enzyme and amino groups on the drugs, with the 1- and 3-amino groups on the 2-DOS ring being particularly important players. It is likely that these interactions will be modulated by the protonation state of the aminogly-

coside. Thus, the pH-dependent chemical properties of the aminoglycosides not only have implications with regard to the specific recognition of designated RNA targets, but also with regard to the recognition of these drugs by modifying enzymes, an interaction that represents a critical step in the primary pathway for aminoglycoside resistance.[17,18]

In addition to the binding-linked protonation effects described above, the studies reported here also provide insights into the molecular forces that contribute to the observed RNA binding free energies exhibited by aminoglycosides in the absence of protonation effects (i.e., at pH 5.5). Using paromomycin as a representative example, we find that the observed RNA binding free energy reflects a balance of two unfavorable and two favorable contributions. The two unfavorable contributions stem from the entropic cost of bimolecular complex formation as well as conformational changes in the RNA required for formation of the drug binding site. These unfavorable energetic contributions are not only balanced, but are overwhelmed by the two favorable contributions, which stem from the polyelectrolyte effect and noncovalent drug–RNA interactions. Between these two favorable contributions to the observed binding free energy, the noncovalent interactions provide the predominant driving force for complex formation, with the polyelectrolyte effect providing a smaller, but still critical, contribution to the binding reaction. Interestingly, the observed RNA binding free energies of the aminoglycosides that we have examined to date (including paromomycin) do not appear to include significant contributions from binding-linked changes in hydration or from the hydrophobic transfer process, the latter observation probably reflecting the polar nature of the aminoglycosides. Our observation that the primary driving force for paromomycin–rRNA complexation appears to be derived from noncovalent drug–RNA interactions suggests that these compounds may be good candidates for structure-based drug design strategies, with the added caveat that any binding-induced conformational changes are well characterized. Such an approach need not be restricted to the addition or removal of polar hydrogen-bond forming groups (e.g., amino and hydroxyl groups), but also of hydrophobic groups (e.g., alkyl and aromatic substituents). However, structural alterations involving hydrophobic groups will change the overall hydrophobicity of the drug and are thus likely to introduce contributions to complex formation from binding-linked changes in hydration as well as from the hydrophobic transfer process. Assessment of the magnitudes of these contributions to observed binding free energies requires thermodynamic measurements, since they are difficult to obtain from structural and computational data alone.

A third significant feature that emerges from thermodynamic studies presented here is a determination of the contributions of specific functional groups to the rRNA binding free energies of the 4,5-disubstituted 2-DOS family of aminoglycosides, which includes neomycin, paromomycin, lividomycin, and ribostamycin. Specifically, we show that ring IV contributes 3.8 kcal/mol to the observed RNA binding free energy, while a 6′-amino vs a 6′-hydroxyl group contributes 1.2 kcal/mol. The magnitudes of these contributions correlate well with the drug–RNA hydrogen-bonding patterns revealed by previously reported[9,14] structural as well as our computational studies. However, it is interesting to note that the correlation between the magnitudes of these contributions to binding free energy and the corresponding contributions to bactericidal activity is not one-to-one. For example, the 3.8 kcal/mol contribution of ring IV translates to a 619-fold enhancement in rRNA binding affinity, but only a 5-fold enhancement in antibacterial activity (unpublished results). These observations suggest that rRNA binding affinity is not the sole modulator of bactericidal activity. It has been suggested that the conformational change in the host RNA induced by the aminoglycosides is responsible for their deleterious effects on protein synthesis and thus their bactericidal activity.[9,14,30,33,74] Whether and how such a conformational change elicits these biological activities represent challenging, but important, questions to be addressed by future studies.

This work was supported, in part, by a grant from the American Cancer Society (RSG-99-153-04-CDD). The calorimetric instrumentation was purchased through funds from NIH grant S10 RR15959-01. DSP was supported, in part, by a Young Investigator Award from the Cancer Institute of New Jersey. We thank Barbara A. Barbieri for her assistance with the osmolality measurements.

REFERENCES

1. Berman, H. M.; Olson, W. K.; Beveridge, D. L.; Westbrook, J.; Gelbin, A.; Demeny, T.; Hsieh, S.-H.; Srinivasan, A. R.; Schneider, B. Biophys J 1992, 63, 751–759.
2. Berman, H. M.; Westbrook, J.; Feng, Z.; Gilliland, G.; Bhat, T. N.; Weissig, H.; Shindyalov, I. N.; Bourne, P. E. Nucleic Acids Res 2000, 28, 235–242.
3. Jiang, F.; Fiala, R.; Live, D.; Kumar, R. A.; Patel, D. J. Biochemistry 1996, 35, 13250–13266.
4. Jiang, L.; Suri, A. K.; Fiala, R.; Patel, D. J. Chem Biol 1997, 4, 35–50.

5. Ye, X.; Gorin, A.; Ellington, A. D.; Patel, D. J. Nature Struct Biol 1996, 3, 1026–1033.
6. Fan, P.; Suri, A. K.; Fiala, R.; Live, D.; Patel, D. J. J Mol Biol 1996, 258, 480–500.
7. Yang, Y.; Kochoyan, M.; Burgstaller, P.; Westhof, E.; Famulok, M. Science 1996, 272, 1343–1346.
8. Jiang, F.; Kumar, R. A.; Jones, R. A.; Patel, D. J. Nature 1996, 382, 183–186.
9. Fourmy, D.; Recht, M. I.; Blanchard, S. C.; Puglisi, J. D. Science 1996, 274, 1367–1371.
10. Patel, D. J.; Suri, A. K.; Jiang, F.; Jiang, L.; Fan, P.; Kumar, R. A.; Nonin, S. J Mol Biol 1997, 272, 645–664.
11. Fourmy, D.; Yoshizawa, S.; Puglisi, J. D. J Mol Biol 1998, 277, 333–345.
12. Jiang, L.; Patel, D. J. Nature Struct Biol 1998, 5, 769–774.
13. Recht, M. I.; Douthwaite, S.; Puglisi, J. D. EMBO J 1999, 18, 3133–3138.
14. Vicens, Q.; Westhof, E. Structure 2001, 9, 647–658.
15. Lynch, S. R.; Puglisi, J. D. J Mol Biol 2001, 306, 1037–1058.
16. Vicens, Q.; Westhof, E. Chem Biol 2002, 9, 747–755.
17. Martin, A. R. In Wilson and Gisvold's Textbook of Organic Medicinal and Pharmaceutical Chemistry, 10th ed.; Delgado, J. N., Remers, W. A., Eds.; Lippincott–Raven Publishers, Philadelphia, PA, 1998; pp 253–325.
18. Kotra, L. P.; Haddad, J.; Mobashery, S. Antimicrob Agents Chemother 2000, 44, 3249–3256.
19. Gutell, R. R. Nucleic Acids Res 1994, 22, 3502–3507.
20. Puglisi, J. D.; Blanchard, S. C.; Dahlquist, K. D.; Easson, R. G.; Fourmy, D.; Lynch, S. R.; Recht, M. I.; Yoshizawa, S. In The Ribosome: Structure, Function, Antibiotics, and Cellular Interactions; Garrett, R. A., Douthwaite, S. R., Liljas, A., Metheson, A. T., Moore, P. B., Noller, H. F., Eds.; ASM Press: Washington, DC, 2000; pp 419–429.
21. Green, R.; Noller, H. F. Annu Rev Biochem 1997, 66, 679–716.
22. Davies, J.; Gorini, L.; Davis, B. D. Mol Pharmacol 1965, 1, 93–106.
23. Davies, J.; Davis, B. D. J Biol Chem 1968, 243, 3312–3316.
24. Dorman, D. E.; Paschal, J. W.; Merkel, K. E. J Am Chem Soc 1976, 98, 6885–6888.
25. Botto, R. E.; Coxon, B. J Am Chem Soc 1983, 105, 1021–1028.
26. Gaggelli, E.; Gaggelli, N.; Maccotta, A.; Valensin, G.; Marini, D.; Di Cocco, M. E.; Delfini, M. Spectrochim Acta Part A 1995, 51, 1959–1963.
27. Kane, R. S.; Glink, P. T.; Chapman, R. G.; McDonald, J. C.; Jensen, P. K.; Gao, H.; Pasa-Tolíc, L.; Smith, R. D.; Whiteside, G. M. Anal Chem 2001, 73, 4028–4036.
28. Kaul, M.; Barbieri, C. M.; Pilch, D. S. J Mol Biol 2003, 326, 1373–1387.
29. Powers, T.; Noller, H. F. RNA 1995, 1, 194–209.
30. Carter, A. P.; Clemons, W. M.; Brodersen, D. E.; Morgan-Warren, R. J.; Wimberly, B. T.; Ramakrishnan, V. Nature 2000, 407, 340–348.
31. Wimberly, B. T.; Brodersen, D. E.; Clemons, W. M. J.; Morgan-Warren, R. J.; Carter, A. P.; Vonrhein, C.; Hartsch, T.; Ramakrishnan, V. Nature 2000, 407, 327–339.
32. Recht, M. I.; Fourmy, D.; Blanchard, S. C.; Dahlquist, K. D.; Puglisi, J. D. J Mol Biol 1996, 262, 421–436.
33. Yoshizawa, S.; Fourmy, D.; Puglisi, J. D. EMBO J 1998, 17, 6437–6448.
34. Jin, E.; Katritich, V.; Olson, W. K.; Kharatisvili, M.; Abagyan, R.; Pilch, D. S. J Mol Biol 2000, 298, 95–110.
35. Kaul, M.; Pilch, D. S. Biochemistry 2002, 41, 7695–7706.
36. Doyle, M. L.; Louie, G.; Dal Monte, P. R.; Sokoloski, T. D. Methods Enzymol 1995, 259, 183–194.
37. Christensen, J. J.; Hansen, L. D.; Izatt, R. M. Handbook of Proton Ionization Heats; John Wiley & Sons, New York, 1976; pp 1–269.
38. Ma, C.; Baker, N. A.; Joseph, S.; McCammon, J. A. J Am Chem Soc 2002, 124, 1438–1442.
39. Hendrix, M.; Priestly, E. S.; Joyce, G. F.; Wong, C. J Am Chem Soc 1997, 119, 3641–3648.
40. Alper, P. B.; Hendrix, M.; Sears, P.; Wong, C.-H. J Am Chem Soc 1998,120, 1965–1978.
41. Fisher, H. F.; Singh, N. Methods Enzymol 1995, 259, 194–221.
42. Haq, I.; Ladbury, J. E.; Chowdhry, B. Z.; Jenkins, T. C.; Chaires, J. B. J Mol Biol 1997, 271, 244–257.
43. Chaires, J. B. Nucleic Acid Sci (Biopolymers) 1998, 44, 201–215.
44. Mazur, S.; Tanious, F. A.; Ding, D.; Kumar, A.; Boykin, D. W.; Simpson, I. J.; Neidle, S.; Wilson, W. D. J Mol Biol 2000, 300, 321–337.
45. Haq, I.; Jenkins, T. C.; Chowdhry, B. Z.; Ren, J.; Chaires, J. B. Methods Enzymol 2000, 323, 373–405.
46. Spolar, R. S.; Livingstone, J. R.; Record, M. T. J. Biochemistry 1992, 31, 3947–3955.
47. Spolar, R. S.; Record, M. T., Jr. Science 1994, 263, 777–784.
48. Sharp, K. A. In Thermodynamics in Biology; Di Cera, E., Ed.; Oxford University Press, New York, 2000; pp. 113–130.
49. Eftink, M. R.; Anusiem, A. C.; Biltonen, R. L. Biochemistry 1983, 22, 3884–3896.
50. Crothers, D. M. Biopolymers 1971, 10, 2147–2160.
51. Doyle, M. L.; Brigham-Burke, M.; Blackburn, M. N.; Brooks, I. S.; Smith, T. M.; Newman, R.; Reff, M.; Stafford, W. F., III; Sweet, R. W.; Truneh, A.; Hensley, P.; O'Shannessy, D. J. Methods Enzymol 2000, 323, 207–230.
52. Record, M. T. J.; Anderson, C. F.; Lohman, T. M. Quart Rev Biophys 1978,11, 103–178.
53. Robinson, C. R.; Sligar, S. G. Methods Enzymol 1995, 259, 395–427.

54. Parsegian, V. A.; Rand, R. P.; Rau, D. C. Methods Enzymol 1995, 259, 43–94.
55. Spink, C. H.; Chaires, J. B. Biochemistry 1999, 38, 496–508.
56. Garner, M. M.; Rau, D. C. EMBO J 1995, 14, 1257–1263.
57. Qu, X.; Chaires, J. B. J Am Chem Soc 2001, 123, 1–7.
58. Westhof, E. Int J Biol Macromol 1987, 9, 186–192.
59. Westhof, E.; Dumas, P.; Moras, D. Biochimie 1988, 70, 145–165.
60. Auffinger, P.; Westhof, E. J Mol Biol 2000, 300, 1113–1131.
61. Atkins, P. W. Physical Chemistry, 3rd ed.; W. H. Freeman and Company: New York, 1986; pp 521–522.
62. Finkelstein, A. V.; Janin, J. Protein Eng 1989, 3, 1–3.
63. Janin, J. Proteins Struct Funct Genet 1996, 24, i–ii.
64. Horton, N.; Lewis, M. Protein Sci 1992, 1, 169–181.
65. Murphy, K. P.; Xie, D.; Thompson, K. S.; Amzel, L. M.; Freire, E. Proteins Struct Funct Genet 1994, 18, 63–67.
66. Suurkuusk, J.; Alvarez, J.; Freire, E.; Biltonen, R. Biopolymers 1977, 16, 2641–2652.
67. Dewey, T. G.; Turner, D. H. Biochemistry 1979, 18, 5757–5762.
68. Park, Y.-W.; Breslauer, K. J. Proc Natl Acad Sci USA 1991, 88, 1551–1555.
69. Ha, J. H.; Spolar, R. S.; Record, M. T. J. J Mol Biol 1989, 209, 801–816.
70. Eftink, M.; Biltonen, R. In Biological Microcalorimetry; Beezer, A. E., Ed.; Academic Press: London, 1980; pp 343–412.
71. Connelly, P. R. Curr Opin Biotechnol 1994, 5, 381–388.
72. Ren, J.; Jenkins, T. C.; Chaires, J. B. Biochemistry 2000, 39, 8439–8447.
73. Fong, D. H.; Berghuis, A. M. EMBO J 2002, 21, 2323–2331.
74. Yoshizawa, S.; Fourmy, D.; Puglisi, J. D. Science 1999, 285, 1722–1725.
75. Fukada, H.; Takahashi, K.; Sturtevant, J. M. Biochemistry 1987, 26, 4063–4068.
76. Fourmy, D.; Recht, M. I.; Puglisi, J. D. J Mol Biol 1998, 277, 347–362.